

# Filtering and analyzing mobile qubit information via Rashba-Dresselhaus-Aharonov-Bohm interferometers

Amnon Aharony,<sup>1,\*</sup> Yasuhiro Tokura,<sup>2</sup> Guy Z. Cohen,<sup>3,†</sup> Ora Entin-Wohlman,<sup>1,†</sup> and Shingo Katsumoto<sup>4</sup>

<sup>1</sup>*Department of Physics and the Ilse Katz Center for Meso- and Nano-Scale Science and Technology, Ben-Gurion University, Beer Sheva 84105, Israel*

<sup>2</sup>*NTT Basic Research Laboratories, NTT Corporation, Atsugi-shi, Kanagawa 243-0198, Japan*

<sup>3</sup>*Department of Physics, Ben-Gurion University, Beer Sheva 84105, Israel*

<sup>4</sup>*Institute of Solid State Physics, University of Tokyo, Kashiwa, Chiba 277-8581, Japan*

(Dated: February 28, 2022)

Spin-1/2 electrons are scattered through one or two diamond-like loops, made of quantum dots connected by one-dimensional wires, and subject to both an Aharonov-Bohm flux and (Rashba and Dresselhaus) spin-orbit interactions. With some symmetry between the two branches of each diamond, and with appropriate tuning of the electric and magnetic fields (or of the diamond shapes) this device completely blocks electrons with one polarization, and allows only electrons with the opposite polarization to be transmitted. The directions of these polarizations are tunable by these fields, and do not depend on the energy of the scattered electrons. For each range of fields one can tune the site and bond energies of the device so that the transmission of the fully polarized electrons is close to unity. Thus, these devices perform as ideal spin filters, and these electrons can be viewed as mobile qubits; the device writes definite quantum information on the spinors of the outgoing electrons. The device can also read the information written on incoming polarized electrons: the charge transmission through the device contains full information on this polarization. The double-diamond device can also act as a realization of the Datta-Das spin field-effect transistor.

PACS numbers: 85.75.Hh, 75.76.+j, 72.25.Dc, 75.70.Tj, 03.65.Vf

Keywords: Spin filter; mobile qubits; spin polarized transport; Rashba and Dresselhaus spin-orbit interactions; Aharonov-Bohm flux; Aharonov-Casher effect; spin field-effect transistor; quantum interference devices.

## I. INTRODUCTION

Future device technology and quantum information processing may be based on spintronics,<sup>1</sup> where one manipulates the electron's spin (and not only its charge). Adding the spin degree of freedom to conventional charge-based electronic devices has the potential advantages of longer decoherence times and lengths, increased data processing speed, lower power consumption, and increased integration densities compared with conventional semiconductor devices. Spins may also be used as qubits in quantum computers.<sup>2</sup> Quantum information is stored in the two complex components of the spinor which represents a spin- $\frac{1}{2}$  state. This information is equivalently contained in the unit vector along which the spin is polarized. Writing and reading information on a spin qubit is thus equivalent to polarizing this spin along a specific direction, and later identifying this direction. Many of the proposed experimental realizations of qubits consider *static* qubits, e.g. an electron localized on a quantum dot.<sup>3-5</sup> With static qubits, the quantum information is transferred via the exchange interactions between the qubits, rather than by the qubits themselves. Here we consider *mobile* qubits:<sup>6,7</sup> the quantum information is carried by polarized spin- $\frac{1}{2}$  particles (e.g. electrons). Mobile qubits were implemented<sup>8</sup> in a two dimensional electron gas (2DEG) using a surface acoustic wave (SAW), that captures individual electrons along its potential minima. Using one SAW, single electrons in parallel quantum 1D channels can be dragged and used as synchronized

inputs to a quantum gate. Although presenting additional constraints for coherence and synchronization, mobile qubits have many advantages over static ones. With mobile qubits, manipulation is done by *static* electric and magnetic fields rather than by expensive high-frequency (scale of giga-Hertz) electromagnetic pulses.<sup>9</sup> Also, using a beam of many electrons enables ensemble averages over the information carried by each of them, reducing the errors.

Mesoscopic *spin filters* (or valves) are devices which polarize the spins going through them along tunable directions, or - equivalently - write quantum information on these mobile qubits. Spin filters can also be used as *spin analyzers*, which read this information by identifying the polarization directions of incoming polarized beams. The present paper discusses such devices. We start with a brief review of alternative approaches. A priori, an elementary way to obtain polarized electrons is to inject them from a ferromagnet,<sup>10</sup> after generating them e.g. optically.<sup>11</sup> Connecting ferromagnets to semiconductors is inefficient, due to a large impedance mismatch between them.<sup>12</sup> Optical generation is difficult to integrate with electronic devices. Another method, which also involves ferromagnets, uses a magnetic tunnel junction,<sup>13-16</sup> with a different tunneling barrier height for each spin direction. The main difficulty is again the impedance match problem between the ferromagnetic junction and the semiconductor at the output. Several proposed filters use quantum dots, in which the filtering is based on either the Coulomb blockade and the Pauli

principle<sup>17–19</sup> or on the Zeeman energy splitting.<sup>20,21</sup> All the above filters usually generate only a *partial* spin polarization. For writing useful quantum information, the outgoing electrons must be *fully* polarized.

Here we follow an alternative early proposal of a spin field-effect transistor (SFET), by Datta and Das,<sup>22</sup> which takes advantage of the spin-orbit interaction (SOI). In vacuum, the SOI has the form<sup>23</sup>

$$\mathcal{H}_{\text{SO}} = \Lambda \boldsymbol{\sigma} \cdot [\mathbf{p} \times \nabla V(\mathbf{r})], \quad (1)$$

where  $\Lambda = \hbar/(2m_0c)^2$  ( $m_0$  is the mass of a free electron,  $c$  is the speed of light),  $\mathbf{p}$  is the electron momentum,  $V(\mathbf{r})$  is the potential and the Pauli matrices  $\boldsymbol{\sigma}$  indicate the electron spin  $\mathbf{s} = \hbar\boldsymbol{\sigma}/2$ . Here we concentrate on mesoscopic structures, made of narrow gap semiconductor heterostructures, in which electrons are confined to move in a plane (the  $xy$ -plane below), forming a 2DEG. In such semiconductors, the microscopic SOI (1) modifies the band structure, and often introduces a spin splitting of bands.<sup>24</sup> The final result can often be written as an effective SOI Hamiltonian, of the general form  $\mathcal{H}_{\text{SO}} = (\hbar/m)(\boldsymbol{\kappa}_{\text{SO}} \cdot \boldsymbol{\sigma})$ , where  $\boldsymbol{\kappa}_{\text{SO}}$  is a linear combination of the electron momentum components  $p_x$  and  $p_y$  and  $m$  is the effective mass, which is usually much smaller than  $m_0$ . The related energy scale can be larger than that of Eq. (1) by as much as six orders of magnitude.

The literature has emphasized two special cases of the effective SOI. A confining potential well which is asymmetric under space inversion generates the Rashba SOI.<sup>25</sup> For an electric field  $\mathbf{E} = -\nabla V$  in the  $z$ -direction, this SOI is similar to Eq. (1):

$$\mathcal{H}_{\text{R}} = \frac{\hbar k_{\text{R}}}{m}(p_y \sigma_x - p_x \sigma_y). \quad (2)$$

The coefficient  $k_{\text{R}}$  typically depends on  $\mathbf{E}$ , as indeed confirmed experimentally.<sup>26–29</sup> When the bulk crystal unit cell lacks inversion symmetry, one also has the Dresselhaus SOI,<sup>30</sup> which is usually cubic in the momentum. For a 2DEG this SOI is given by

$$\mathcal{H}_{\text{D}} = \frac{\hbar k_{\text{D}}}{m}(p_x \sigma_x - p_y \sigma_y), \quad (3)$$

where  $k_{\text{D}}$  usually depends on the crystal structure and only weakly (if at all) on the external field. From the strictly theoretical point of view, however, there is not much difference between the linear Dresselhaus interaction and the Rashba term, as they are connected by a unitary transformation.<sup>31</sup> A similar transformation can also switch the sign of the second term in (3). For the purposes of the present paper we shall keep the generic separation between  $\mathcal{H}_{\text{R}}$  and  $\mathcal{H}_{\text{D}}$ .

When a spin moves a distance  $L$  in the direction of the unit vector  $\hat{\mathbf{g}}$  then its spinor  $|\chi\rangle$  transforms into  $|\chi\rangle \rightarrow U|\chi\rangle$ , with the unitary spin rotation matrix<sup>32</sup>

$$U = e^{i\mathbf{K} \cdot \boldsymbol{\sigma}}, \quad \mathbf{K} = \alpha_{\text{R}}(g_y, -g_x, 0) + \alpha_{\text{D}}(g_x, -g_y, 0), \quad (4)$$

with  $\alpha_{\text{R,D}} = k_{\text{R,D}}L$ . The Datta-Das SFET used this effect to rotate the spins of electrons which move in a quasi-one-dimensional semiconductor wire, connected to two ferromagnets. Experimental realizations of this device are still awaiting the solution of the impedance matching problem. From now on we discuss filters which avoid ferromagnets. In a 2DEG with SOI, an interface between two regions with different SOI's causes a splitting of each beam into two polarized beams with different velocities. This was the basis for the refraction/reflection filter.<sup>33–35</sup> Another SOI based filter uses mesoscopic T junctions, which split the unpolarized electron beam into two polarized ones.<sup>36–39</sup> These filters are advantageous since they produce two polarized beams, thus using all the electrons in the original beam, and since they do not use magnetic fields. However, the outgoing polarization depends on the electrons' energy. In most of this paper we calculate the transmission of electrons, moving from a left lead to a right lead via a scattering device, the 'filter'. However, at the end we also mention the conductance between two unpolarized reservoirs which are connected to these leads, and then one may need to average the polarization of electrons with different energies, e.g. at finite temperature and/or finite bias voltage. It is thus advantageous to have *energy-independent* polarizations.

The filters discussed below take advantage of the *interference of electronic waves in quantum networks* which contain closed loops. The phases of these waves can include the Aharonov-Bohm (AB) phase  $\phi$ ,<sup>40</sup> which results from a magnetic flux  $\Phi$  penetrating each loop. When an electron goes around a loop its wave functions gains an AB phase  $\phi \equiv 2\pi\Phi/\Phi_0$ , and  $\Phi_0 = hc/e$  is the unit flux ( $e$  is the electron charge). This phase is a special example of the Berry phase.<sup>41</sup> Another example involves the Aharonov-Casher effect,<sup>42</sup> which is related to the spin degree of freedom. When an electron goes around a loop along which it is subject to the SOI, its spinor rotates by the transformation

$$u = \exp[i\boldsymbol{\omega} \cdot \boldsymbol{\sigma}] \equiv \cos \omega + i \sin \omega \hat{\mathbf{m}}, \quad (5)$$

where  $\hat{\mathbf{m}} \equiv \boldsymbol{\omega}/\omega$ , introducing an additional SOI-related phase  $\omega = |\boldsymbol{\omega}|$ . The matrix  $u$  is a product of matrices of the kind given in Eq. (4), each coming from the local SOI on a segment of the loop. As indicated by Eq. (4), this matrix depends on the geometric details of the bonds around the loop (unlike  $\phi$ , which only depends on the area of the loop). Indeed, many papers proposed a single circular loop interferometer which would be sensitive to this phase and/or to its competition with the AB phase.<sup>32,43–51</sup> The loop is connected to two leads, and the destructive interference of the waves in the two paths can sometimes block electrons with one polarization, and fully transmit electrons with the opposite polarization. Some papers also suggested to connect the loop to three leads, as in a Stern-Gerlach experiment.<sup>52,53</sup> However, the calculated criteria for filtering in these papers were usually energy-dependent, and there was no systematic discussion of these criteria and of the polarization of the

transmitted spins. An alternative geometry replaces the circular loop by a diamond-shaped square, with a SOI on its four edges (which determine  $\omega$ ) and with a penetrating AB flux, see Fig. 1.<sup>51,54</sup> Indeed, these papers find criteria for full spin filtering, but restrict their discussion to isolated values of the AB flux and the SOI. Below we generalize these pioneering results in many directions.

Interference becomes simpler in the Mach-Zhender mesoscopic interferometer, which imitates the two-slit experiment.<sup>55–59</sup> Reference 59 found an energy-independent criterion (which relates the SOI strength and the AB flux) for full spin polarization and an energy-independent polarization direction, similar to those discussed below. Since the Mach-Zhender interferometer requires two beam splitters, which may not be easy to realize, we consider mainly simple interferometers, based on one or two loops. Networks of rings have also been considered, with SOI and (sometimes) with an AB flux.<sup>29,60–64</sup> In particular, an infinite network of diamond-shaped rings<sup>62,63</sup> was found to give a wide range of electric and magnetic fields with full polarization at the output. Since infinite networks are difficult to realize, we discuss here only the cases of one and two diamonds.

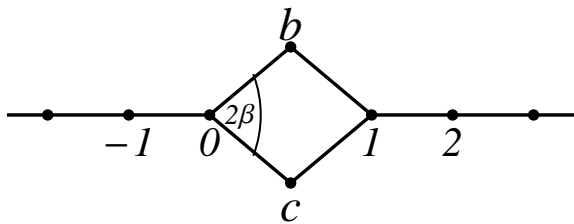


FIG. 1: The single diamond and the leads. The diamond is penetrated by a magnetic flux  $\Phi$ , and the bonds around it are subject to SOI's.

In this paper we avoid some of the problems listed above. Using scattering theory, we calculate the spin-dependent transmission through a single and a double diamond-like loops (Figs. 1 and 2). We allow for general opening angles of the diamond rhombi,  $\{2\beta_i\}$ , which affect both the SOI, via the lengths and orientations of the bonds, and the AB flux, via the diamond area. We also include both the Rashba and the Dresselhaus SOI, in addition to the AB flux. The Dresselhaus SOI depends on the relative rotation of the crystal axes and the diamond bonds, see Fig. 3. For a fixed value of  $k_D$  we find explicit and relatively simple relations between  $\phi$ ,  $k_R$  and the  $\beta$ 's, at which the transmitted electrons are fully polarized in tunable directions which we calculate. These relations and the spin polarizations do not depend on the energy of the electrons. The transmission coefficient of these polarized electrons can be tuned to be very close to unity. The transmission of electrons with other polarizations is smaller, and can be used for 'reading' their polarization.

Section II discusses the single-diamond case, Fig. 1. We first present a general calculation of the the transmission through the diamond, valid for any internal structure

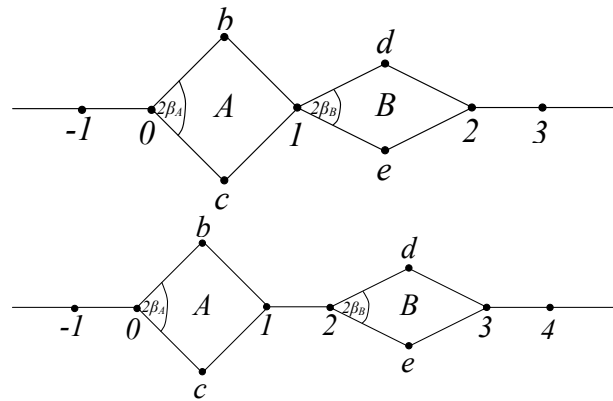


FIG. 2: Schematic diagrams of the two-diamond filters.

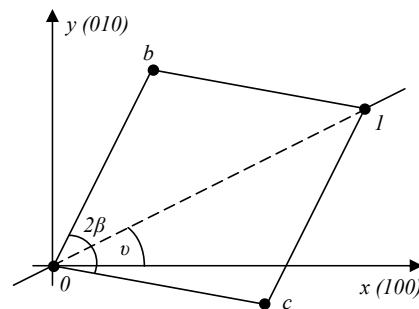


FIG. 3: Schematic diagram of the rotated diamond, in the presence of the Dresselhaus SOI. The  $x$  and  $y$  axes are set at the crystal axes of the material.

of the two one-dimensional paths (Subsec. IIA), find the general conditions for full filtering and for using the filter as an analyzer (IIB), and then find specific criteria for the Rashba-only SOI (IIC) and for both Rashba and Dresselhaus SOI's (IID). Section III discusses two diamonds in series, as in Fig. 2, (IIIA) and gives explicit expressions for special cases which can yield full filtering with a transmission of unity for practically all energies (IIIB). The results are discussed and summarized in Sec. IV.

## II. A SINGLE DIAMOND

### A. Transmission of an arbitrary diamond

We start with the scattering of an electron from a diamond with arbitrary SOI and AB flux. Consider an electron with spin  $\frac{1}{2}$ , moving on a general network of sites. The tight-binding Schrödinger equation for the spinor  $|\psi(u)\rangle$  at site  $u$  is written as

$$(\epsilon - \epsilon_u)|\psi(u)\rangle = - \sum_v \tilde{U}_{uv} |\psi(v)\rangle, \quad (6)$$

where  $v$  runs over the nearest neighbors of  $u$ , while  $\tilde{U}_{uv} \equiv J_{uv}U_{uv}$ ,  $J_{uv}$  is a hopping energy and  $U_{uv}$  is a  $2 \times 2$  unitary matrix. For the diamond in Fig. 1, the matrices  $U_{uv}$  differ from the  $2 \times 2$  unit matrix  $\mathbf{1}$  only for the four bonds forming the diamond. At this stage we do not specify the details of these four matrices, which contain the AB phase and the SOI rotation, or of the corresponding four coefficients  $J_{uv}$ .

Except for the above four bonds, the nearest neighbor hopping energy along the leads is  $j$ , with no spin-orbit interaction, and the site energies  $\epsilon_u$  on the leads are zero. With a lattice constant  $a$ , the states on the leads are combinations of  $e^{\pm i n k a}$ , multiplying  $n$ -independent spinors, and the corresponding energy is  $\epsilon = -2j \cos(ka)$ . The Schrödinger equations for the spinors at the corners of the diamond are

$$\begin{aligned} (\epsilon - \epsilon_0)|\psi(0)\rangle &= -(\tilde{U}_{0b}|\psi(b)\rangle + \tilde{U}_{0c}|\psi(c)\rangle) - j|\psi(-1)\rangle, \\ (\epsilon - \epsilon_1)|\psi(1)\rangle &= -(\tilde{U}_{b1}^\dagger|\psi(b)\rangle + \tilde{U}_{c1}^\dagger|\psi(c)\rangle) - j|\psi(2)\rangle, \\ (\epsilon - \epsilon_b)|\psi(b)\rangle &= -(\tilde{U}_{0b}^\dagger|\psi(0)\rangle + \tilde{U}_{b1}|\psi(1)\rangle), \\ (\epsilon - \epsilon_c)|\psi(c)\rangle &= -(\tilde{U}_{0c}^\dagger|\psi(0)\rangle + \tilde{U}_{c1}|\psi(1)\rangle). \end{aligned} \quad (7)$$

Substituting the last two equations into the first two, one has

$$\begin{aligned} (\epsilon - y_0)|\psi(0)\rangle &= \mathbf{W}|\psi(1)\rangle - j|\psi(-1)\rangle, \\ (\epsilon - y_1)|\psi(1)\rangle &= \mathbf{W}^\dagger|\psi(0)\rangle - j|\psi(2)\rangle, \end{aligned} \quad (8)$$

where

$$y_u \equiv \epsilon_u + \gamma_{ubu} + \gamma_{ucu}, \quad \gamma_{uvw} \equiv J_{uv}J_{vw}/(\epsilon - \epsilon_v), \quad (9)$$

$$\mathbf{W} \equiv \gamma_{0b1}U_{0b}U_{b1} + \gamma_{0c1}U_{0c}U_{c1}. \quad (10)$$

Generally,  $\mathbf{W}$  is not a unitary matrix (unlike the  $U$ 's). Like any  $2 \times 2$  matrix,  $\mathbf{W}$  can always be written as

$$\mathbf{W} = d + \mathbf{b} \cdot \boldsymbol{\sigma}, \quad (11)$$

where  $d$  and  $\mathbf{b}$  are a complex number and a complex three-component vector, which are determined by the details of the hopping matrices  $U_{uv}$ .

A wave coming from the left has the form

$$\begin{aligned} |\psi(n)\rangle &= e^{ikna}|\chi_{in}\rangle + re^{-ikna}|\chi_r\rangle, \quad n \leq 0, \\ |\psi(n)\rangle &= te^{ik(n-1)a}|\chi_t\rangle, \quad n \geq 1, \end{aligned} \quad (12)$$

where  $|\chi_{in}\rangle$ ,  $|\chi_r\rangle$  and  $|\chi_t\rangle$  are the incoming, reflected and transmitted normalized spinors, respectively (with the corresponding reflection and transmission complex amplitudes  $r$  and  $t$ ). Substituting Eqs. (12) into Eqs. (8) one finds

$$t|\chi_t\rangle = \mathcal{T}|\chi_{in}\rangle, \quad r|\chi_r\rangle = \mathcal{R}|\chi_{in}\rangle, \quad (13)$$

with the  $2 \times 2$  transmission and reflection amplitude matrices

$$\mathcal{T} = 2ij \sin(ka) \mathbf{W}^\dagger (\mathbf{Y}\mathbf{1} - \mathbf{W}\mathbf{W}^\dagger)^{-1}, \quad (14)$$

$$\mathcal{R} = -\mathbf{1} - 2ij \sin(ka) X_1 (\mathbf{Y}\mathbf{1} - \mathbf{W}\mathbf{W}^\dagger)^{-1}. \quad (15)$$

Here,

$$Y = X_0 X_1, \quad X_u = y_u + j e^{-ika}. \quad (16)$$

Both  $\mathcal{T}$  and  $\mathcal{R}$  involve the hermitian matrix

$$\mathbf{W}\mathbf{W}^\dagger = A + \mathbf{B} \cdot \boldsymbol{\sigma}, \quad (17)$$

where [by Eq. (11)]

$$\begin{aligned} A &= |d|^2 + \mathbf{b} \cdot \mathbf{b}^*, \\ \mathbf{B} &= 2\text{Re}[d^* \mathbf{b}] + 2[\text{Re}(\mathbf{b}) \times \text{Im}(\mathbf{b})] \equiv |\mathbf{B}|\hat{\mathbf{n}}. \end{aligned} \quad (18)$$

Defining the eigenstate of the spin component along a general unit vector  $\hat{\mathbf{n}}$  via  $\hat{\mathbf{n}} \cdot \boldsymbol{\sigma}|\hat{\mathbf{n}}\rangle = |\hat{\mathbf{n}}\rangle$ , the eigenvectors of  $\mathbf{W}\mathbf{W}^\dagger$  are identified as  $|\pm \hat{\mathbf{n}}\rangle$ ,

$$\mathbf{W}\mathbf{W}^\dagger|\pm \hat{\mathbf{n}}\rangle = \lambda_\pm|\pm \hat{\mathbf{n}}\rangle, \quad \lambda_\pm = A \pm |\mathbf{B}|. \quad (19)$$

Equation (10) presents an example of the general two-path loop, for which one can write

$$\mathbf{W} = \gamma_b U_b + \gamma_c U_c, \quad (20)$$

with real coefficients  $\gamma_b$  and  $\gamma_c$  and with unitary matrices  $U_b$  and  $U_c$  corresponding to the two paths. The same form (20) is found when each path contains a chain of many bonds in series.<sup>63</sup> This form yields

$$\mathbf{W}\mathbf{W}^\dagger = \gamma_b^2 + \gamma_c^2 + \gamma_b \gamma_c (u + u^\dagger), \quad (21)$$

where  $u \equiv U_b U_c^\dagger$  is the unitary matrix representing hopping from 0 back to 0 around the loop.<sup>51</sup> As discussed in the introduction, this matrix has the form  $u = e^{-i\phi + i\boldsymbol{\omega} \cdot \boldsymbol{\sigma}}$ , see Eq. (5) and preceding discussion. Thus,  $u + u^\dagger = 2(\cos \omega \cos \phi + \sin \omega \sin \phi \hat{\mathbf{m}} \cdot \boldsymbol{\sigma})$ , and one identifies  $\hat{\mathbf{m}} = \hat{\mathbf{n}}$  and

$$\begin{aligned} A &= \gamma_b^2 + \gamma_c^2 + 2\gamma_b \gamma_c \cos \omega \cos \phi, \\ \mathbf{B} &= 2\gamma_b \gamma_c \sin \omega \sin \phi \hat{\mathbf{n}}. \end{aligned} \quad (22)$$

The eigenvalues  $\lambda_\pm$  now become

$$\lambda_\pm = A \pm |\mathbf{B}| = \gamma_b^2 + \gamma_c^2 + 2\gamma_b \gamma_c \cos(\phi \pm \omega). \quad (23)$$

The corresponding eigenstates,  $|\pm \hat{\mathbf{n}}\rangle$ , represent electrons which are fully polarized along  $\pm \hat{\mathbf{n}} = \pm \mathbf{B}/|\mathbf{B}|$ . The direction of  $\hat{\mathbf{n}}$  depends on the sign of  $\sin \omega \sin \phi$ , namely on the directions of the magnetic field (determining the sign of  $\phi$ ) and of the electric field (determining the sign of  $\omega$  in the Rashba case). Switching the sign of  $\phi$  or of  $\omega$  switches the direction of the polarized spins associated with the two eigenvalues.

Equation (15) implies that an incoming spinor  $|\pm \mathbf{n}\rangle$  will generate an outgoing spinor

$$t|\chi_\pm^{out}\rangle = \mathcal{T}|\pm \mathbf{n}\rangle = \frac{2ij \sin(ka)}{Y - \lambda_\pm} \mathbf{W}^\dagger|\pm \mathbf{n}\rangle. \quad (24)$$

Since the scalar product of  $\mathbf{W}^\dagger|\pm\mathbf{n}\rangle$  with itself equals  $\lambda_\pm$ , it follows that

$$|\chi_\pm^{out}\rangle = \mathbf{W}^\dagger|\pm\mathbf{n}\rangle/\sqrt{\lambda_\pm}, \quad (25)$$

and that the corresponding transmission amplitude is

$$t_\pm = \frac{2ij\sin(ka)}{Y - \lambda_\pm}\sqrt{\lambda_\pm}, \quad (26)$$

which is an eigenvalue of  $\mathcal{T}$ .

Equation (25) also implies the relation  $\mathbf{W}^\dagger\mathbf{W}|\chi_\pm^{out}\rangle = \lambda_\pm|\chi_\pm^{out}\rangle$ , showing that  $|\chi_\pm^{out}\rangle$  is an eigenstate of

$$\mathbf{W}^\dagger\mathbf{W} = A + \mathbf{B}' \cdot \boldsymbol{\sigma}, \quad (27)$$

where

$$\mathbf{B}' = 2\text{Re}[d^*\mathbf{b}] - 2[\text{Re}(\mathbf{b}) \times \text{Im}(\mathbf{b})] \equiv |\mathbf{B}|\hat{\mathbf{n}}'. \quad (28)$$

Therefore,  $|\chi_\pm^{out}\rangle$  corresponds to a spin direction  $\hat{\mathbf{n}}'$ , which differs from  $\hat{\mathbf{n}}$  in that the component along  $[\text{Re}(\mathbf{b}) \times \text{Im}(\mathbf{b})]$  is reversed. One can thus identify  $|\pm\hat{\mathbf{n}}'\rangle$  as the left eigenstates of  $\mathbf{W}^\dagger$ , namely

$$\mathbf{W}^\dagger \equiv \sqrt{\lambda_-}|- \mathbf{n}'\rangle\langle -\mathbf{n}| + \sqrt{\lambda_+}|\hat{\mathbf{n}}'\rangle\langle \hat{\mathbf{n}}|. \quad (29)$$

Similarly,

$$\mathcal{T} \equiv t_-|- \mathbf{n}'\rangle\langle -\mathbf{n}| + t_+|\hat{\mathbf{n}}'\rangle\langle \hat{\mathbf{n}}|. \quad (30)$$

Scattering from the right lead to the left lead is obtained by replacing  $\mathbf{W}^\dagger$  by  $\mathbf{W}$ . It follows that an electron polarized along  $\hat{\mathbf{n}}'$  coming from the right hand side (RHS) exits to the left hand side (LHS) polarized along  $\hat{\mathbf{n}}$ . It is now straightforward to find the transmission and reflection matrices  $\mathcal{T}'$  and  $\mathcal{R}'$  for this reversed scattering: all one needs to do is interchange  $\mathbf{W}$  with  $\mathbf{W}^\dagger$  and  $X_0$  with  $X_1$ . Note that generally  $\mathcal{T}' \neq \mathcal{T}$ ; these matrices are related to each other via the self-duality of the scattering matrix.<sup>65</sup> It is then straightforward to check unitarity, e.g.  $\mathcal{T}'^\dagger\mathcal{T} + \mathcal{R}'^\dagger\mathcal{R}' = \mathbf{1}$ .

## B. Ideal filter and reader

Many earlier papers considered the polarization of the moving electrons along a particular fixed direction, e.g. along the  $z$ -axis. Following e.g. Ref. 51, we find it much better to consider the polarization along a *tilted* direction, associated with the eigenstates of the matrix  $\mathbf{W}\mathbf{W}^\dagger$  [or, equivalently, of the matrix  $u + u^\dagger$ , Eq. (21)]. A general incoming spinor  $|\chi_{in}\rangle$  can be expanded in terms of these basis eigenvectors,

$$|\chi_{in}\rangle = c_+|\hat{\mathbf{n}}\rangle + c_-|-\hat{\mathbf{n}}\rangle, \quad (31)$$

with  $c_\pm = \langle \pm\hat{\mathbf{n}}|\chi_{in}\rangle$ , and then the outgoing spinor becomes

$$t|\chi_t\rangle = c_+t_+|\hat{\mathbf{n}}'\rangle + c_-t_-|-\hat{\mathbf{n}}'\rangle. \quad (32)$$

The total charge transmission is therefore  $T = |c_+|^2T_+ + |c_-|^2T_-$ , with  $T_\pm \equiv |t_\pm|^2$  being the eigenvalues of  $\mathcal{T}\mathcal{T}^\dagger$ . Given Eqs. (23) and (26),  $T_\pm$  is a function of  $\phi \pm \omega$ .<sup>43</sup> Note that  $t_\pm$  and  $T_\pm$  are the eigenvalues of  $\mathcal{T}$  and of  $\mathcal{T}\mathcal{T}^\dagger$ , respectively.

The single diamond described above can serve as a perfect filter if one of the eigenvalues  $\lambda_\pm$ , say  $\lambda_-$ , vanishes. In the following sections we show that there exist physical parameters for which this can be achieved - independently of the electron energy  $\epsilon$ . Indeed, if  $\lambda_- = 0$  then one also has  $t_- = 0$ , and Eq. (32) reduces to  $t|\chi_t\rangle = c_+t_+|\hat{\mathbf{n}}'\rangle$ . All outgoing electrons are then polarized along  $\hat{\mathbf{n}}'$ , and the total transmission strength, i.e. the fraction of the incoming current which exits on the RHS, is given by  $T = T_+|c_+|^2$ .

From Eq. (23) it follows that  $\lambda_\pm \geq 0$ , and that the equality  $\lambda_- = 0$  can occur *only* if

$$\gamma_b = \gamma_c \equiv \gamma \quad \text{and} \quad \cos(\phi - \omega) = -1. \quad (33)$$

The first relation implies a symmetry between the two paths. For the specific diamond geometry of Fig. 1, one has  $\gamma_v \equiv \gamma_{0v1}$  [see Eqs. (9) and (10)]. If one imposes the symmetric relation  $J_{0b}J_{b1} = J_{0c}J_{c1}$ , then this condition requires  $\epsilon_b = \epsilon_c$ . Both the  $J$ 's and the  $\epsilon_u$ 's can be tuned via appropriate gate voltages, so that the equality  $\gamma_b = \gamma_c$  can be achieved. The second condition in Eq. (33), namely  $\omega = \phi + \pi$ , yields a relation between the AB flux and the SOI strength (represented by  $\omega$ ). Note that  $\phi$  and  $\omega$  depend only on the unitary matrices  $U_{uv}$ , and *not* on the energy  $\epsilon$  nor on the site energies  $\epsilon_u$ . Also, the vectors  $\hat{\mathbf{n}}$  and  $\hat{\mathbf{n}}'$  depend only on the parameters in these matrices. Thus, for fixed diamond parameters which obey the above conditions the direction of the outgoing electrons' polarization is independent of the energy, and remains the same even after summation over energies due to finite temperature or bias voltage (see below).

Substituting  $\omega = \phi + \pi$  and  $\gamma_b = \gamma_c = \gamma$  in Eq. (23) yields

$$\lambda_+ = 4\gamma^2 \sin^2 \phi. \quad (34)$$

This result for  $\lambda_+(\epsilon)$  is *universal*, in the sense that it depends on the parameters of the diamond only through the AB flux, and *not* on the angle of opening  $\beta$  (Fig. 1) nor on the SOI strengths  $k_R$  and  $k_D$ . Of course, these latter parameters still need to be adjusted by Eq. (33) to achieve full polarization. Having satisfied Eq. (33), the transmission becomes [Eq. (26)]

$$T_+(\epsilon) = \frac{4j^2 \sin^2(ka)\lambda_+}{P + Q \cos(ka) + R \cos(2ka)}, \quad (35)$$

where

$$\begin{aligned} P &= (y_0y_1 - \lambda_+)^2 + (y_0 + y_1)^2j^2 + j^4, \\ Q &= 2j(y_0y_1 - \lambda_+ + j^2)(y_0 + y_1), \\ R &= 2j^2(y_0y_1 - \lambda_+), \end{aligned} \quad (36)$$

and one can read the transmission from graphs of  $T_+$  as function of  $\phi$  and  $\epsilon$ . When  $\sin \phi = 0$  both  $\lambda_+$  and  $\lambda_-$  vanish when also  $\omega = \pi$ , and *all* the electrons are fully reflected. Therefore, one needs  $\sin \phi \neq 0$ , i.e. a non-zero magnetic field. However, as we show below, one can achieve good filtering even for small magnetic fields.

Although all these results are specific for the tight-binding model, one would like to apply them for general leads, with general dispersion relations. For this purpose, it is customary to calculate the tight-binding transmission for energies near the center of the band,  $\epsilon = 0$  or  $ka = \pi/2$ , where the density of states is flat. Equation (34) shows that (for  $\phi \neq 0$ )  $\lambda_+$  diverges as  $\gamma^2 \propto (\epsilon - \epsilon_b)^{-2}$  at the resonant energy  $\epsilon = \epsilon_b$ . This yields a Fano-like zero of  $T_+$  for this energy. Since we prefer to have a weak energy dependence around  $\epsilon = 0$ , it is preferable to have a non-zero (and large) site energy  $\epsilon_b$ .

From now on we set  $J_{uv} \equiv J$ , so that also  $\gamma_{0v0} = \gamma_{1v1} = \gamma$  for  $v = b, c$  [see Eq. (9) and Fig. 1]. At the band center ( $\epsilon = 0$  or  $ka = \pi/2$ ), we also have  $\gamma \rightarrow \gamma_0 = -J^2/\epsilon_b$ , and the denominator in Eq. (35) becomes  $P-R = [(\epsilon_0 + 2\gamma_0)(\epsilon_1 + 2\gamma_0) - \lambda_+ - j^2]^2 + j^2(\epsilon_0 + \epsilon_1 + 4\gamma_0)^2$ , which is minimal at  $\epsilon_0 = \epsilon_1 = -2\gamma_0 \equiv 2J^2/\epsilon_b$ . In this case one has  $T_+ = 4j^2\lambda_+/(\lambda_+ + j^2)^2$ , and this has its maximal value of 1 at  $\lambda_+ = j^2$ . For a specific filter one would usually decide over what range of flux  $\phi$  one would like to work. Fixing  $j$  and  $J_{uv} = J$  and denoting the middle of that range of  $\phi$  by  $\phi_0$ , one has  $T_+ = 1$  at  $\phi = \phi_0$  if one tunes the parameters so that  $\gamma = \gamma_0 = j/(2\sin \phi_0)$ , and  $\epsilon_b = -J^2/\gamma_0$ ,  $\epsilon_0 = \epsilon_1 = -2\gamma_0$ . For these choices, one ends up with

$$T_+(\epsilon = 0) = 4 \sin^2 \phi \sin^2 \phi_0 / (\sin^2 \phi + \sin^2 \phi_0)^2, \quad (37)$$

depending only on  $\phi_0$ , as shown on the LHS of Fig. 4.  $T_+(0)$  has a reasonably flat maximum at  $\phi = \phi_0$  (and a width which increases with  $\phi_0$ ). The other panel in Fig. 4 shows  $T_+$  versus  $ka$  for the flux fixed at  $\phi = \phi_0$ , for the site energies chosen above and for  $J = 4j$ . As expected,  $T_+$  is practically energy-independent and equal to unity in a range around the band center  $ka = \pi/2$ . The width of these plateaus increases with increasing  $J$ , when  $|\epsilon_b| = J^2/|\gamma_0| \gg |\epsilon|$ .

If the incoming electrons are polarized along a direction  $\hat{\mathbf{n}}_0$ , namely  $|\chi_{in}\rangle \equiv |\hat{\mathbf{n}}_0\rangle$ , then one has [Eq. (31)]

$$|c_+|^2 = |\langle \hat{\mathbf{n}} | \hat{\mathbf{n}}_0 \rangle|^2 = \frac{1}{2}(1 + \hat{\mathbf{n}}_0 \cdot \hat{\mathbf{n}}). \quad (38)$$

Thus, the charge transmission through the filter will decrease from  $T_+(\epsilon)$ , when  $\hat{\mathbf{n}}_0 = \hat{\mathbf{n}}$ , to zero, when  $\hat{\mathbf{n}}_0 = -\hat{\mathbf{n}}$ . The relative magnitude of this transmission,  $T(\epsilon)/T_+(\epsilon) = |c_+|^2$  is a linear combination of the components of  $\hat{\mathbf{n}}_0$ , which can thus be extracted by measurements at three pre-tuned values of  $\hat{\mathbf{n}}$ . This amounts to a *reading* of the polarization of the incoming electrons, namely of the quantum information stored in these mobile qubits. If the incoming electrons are not fully polarized, the measured charge transmission will yield information on the average over  $|c_+|^2$ . Specifically, for random

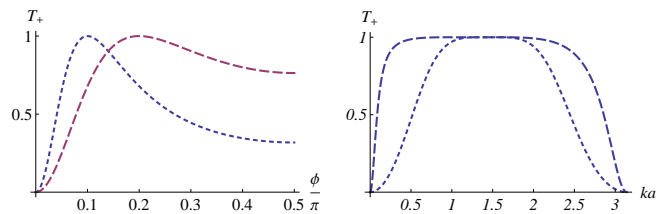


FIG. 4: The transmission of the polarized electrons,  $T_+(\epsilon)$ . LHS: in the band center ( $\epsilon = 0$ ) versus the AB flux  $\phi$  (in units of  $\pi$ ). RHS: versus  $ka$  [the electron energy is  $\epsilon = -2j \cos(ka)$ ], for hopping strengths around the diamond  $J_{uv} = J = 4j$  and site energies  $\epsilon_0 = \epsilon_1 = -j/\sin \phi_0$ ,  $\epsilon_b = \epsilon_c = -2J^2 \sin \phi_0/j$ . These site energies are chosen so that  $T_+$  is maximal at  $\phi = \phi_0$ . Small (large) dashes correspond to maxima of  $T_+(0)$  at  $\phi_0 = .1\pi$  ( $.2\pi$ ).

polarizations one has  $T = T_+/2$ . An alternative way to test the polarization of the outgoing spins is to send them through another filter, see Subsec. IIIB.

### C. Single diamond with Rashba SOI

For specific types of interaction one needs explicit forms for the unitary hopping matrices  $U_{uv}$ . Consider a bond of length  $L$  from  $\mathbf{r}_u$  to  $\mathbf{r}_v$ , with  $\mathbf{r}_v - \mathbf{r}_u \equiv L\hat{\mathbf{g}}_{uv}$ . Placing the magnetic field  $\mathbf{H}$  along the  $z$  direction and choosing the gauge  $\mathbf{A} = \frac{1}{2}\mathbf{H} \times \mathbf{r}$ , we assign an AB phase  $\phi_{uv}$  to  $U_{uv}$ :

$$\phi_{uv} = \frac{\pi HL}{\Phi_0} [\hat{\mathbf{g}}_{uv} \times \hat{\mathbf{z}}] \cdot \mathbf{r}_u. \quad (39)$$

With the SOI, one has  $U_{uv} = \exp[i\phi_{uv} + i\mathbf{K}_{uv} \cdot \boldsymbol{\sigma}]$ , and  $\mathbf{K}_{uv}$  is given by Eq. (4) with  $\hat{\mathbf{g}} \rightarrow \hat{\mathbf{g}}_{uv}$ . To demonstrate the power of our formalism, we start here by considering only the Rashba SOI. Generalizing Ref. 51, our diamond is a rhombus with an opening angle of  $2\beta$ . Choosing the  $x$ -axis along the leads, the four sites of the diamond are at  $\mathbf{r}_0 = (0, 0, 0)$ ,  $\mathbf{r}_b = (L \cos \beta, L \sin \beta, 0)$ ,  $\mathbf{r}_c = (L \cos \beta, -L \sin \beta, 0)$  and  $\mathbf{r}_1 = (2L \cos \beta, 0, 0)$  (Fig. 1). The hopping matrices for the four bonds then become

$$\begin{aligned} U_{0b} &= \exp(i\alpha\sigma_1), & U_{b1} &= \exp(-i\phi/2 - i\alpha\sigma_2), \\ U_{0c} &= \exp(-i\alpha\sigma_2), & U_{c1} &= \exp(i\phi/2 + i\alpha\sigma_1), \end{aligned} \quad (40)$$

where  $\alpha = \alpha_R = k_R L \equiv \alpha_1/\cos \beta$ ,  $\sigma_1 = \sin \beta \sigma_x - \cos \beta \sigma_y$ ,  $\sigma_2 = \sin \beta \sigma_x + \cos \beta \sigma_y$  and  $\phi/(2\pi) = HL^2 \sin(2\beta)/\Phi_0 \equiv \phi_1 \tan \beta$  is the number of flux units through the diamond. In these expressions we have introduced

$$\alpha_1 = k_R L_0, \quad \phi_1 = 2HL_0^2/\Phi_0, \quad (41)$$

where  $2L_0$  is the distance between sites 0 and 1. These parameters do not depend on  $\beta$  even when the sites  $b$  and  $c$  are moved in order to vary  $\beta$  (see below). Substituting

the matrices (40) into Eq. (10) one obtains Eq. (11), with

$$\begin{aligned} d &= a_+[c^2 - s^2 \cos(2\beta)], & b_x &= 0, \\ b_y &= -2ia_+cs \cos \beta, & b_z &= ia_-s^2 \sin(2\beta), \end{aligned} \quad (42)$$

where  $c = \cos \alpha$ ,  $s = \sin \alpha$  and

$$a_{\pm} = \gamma_b e^{-i\phi/2} \pm \gamma_c e^{i\phi/2}. \quad (43)$$

Equation (18) now reproduces Eq. (22), with the identification  $\cos \omega = 1 - 2s^4 \sin^2(2\beta)$  and  $\sin \omega = 2s^2 \sin(2\beta) \sqrt{1 - s^4 \sin^2(2\beta)}$ . For  $\beta = \pi/4$  this value of  $\omega$  was found in Ref. 51. Also,

$$\hat{\mathbf{n}} = s_{\phi} (2cs \cos \beta, 0, c^2 - s^2 \cos(2\beta)) / \sqrt{1 - s^4 \sin^2(2\beta)}, \quad (44)$$

where  $s_{\phi} = \text{sign}[\sin \phi]$ . Below we present results for  $s_{\phi} > 0$ . Furthermore, Eq. (28) gives

$$\hat{\mathbf{n}}' = (-\hat{n}_x, 0, \hat{n}_z). \quad (45)$$

The condition (33) now implies that

$$\cos(\phi/2) = \pm \sin^2 \alpha \sin(2\beta). \quad (46)$$

This equation corresponds to a line in the  $\phi$ - $\alpha$  plane, which is shown in Fig. 5 (for three values of  $\beta$ ). If one varies both  $\alpha$  and  $\phi$  along such a line, then the outgoing spins are fully polarized, and the transmission is given by Eq. (35). One should note that  $\phi = 2\pi\phi_1 \tan \beta$  and  $\alpha = \alpha_1 / \cos \beta$ , and these relations should be taken into account when translating  $\phi$  and  $\alpha$  to the magnetic and electric fields for different angles  $\beta$ .

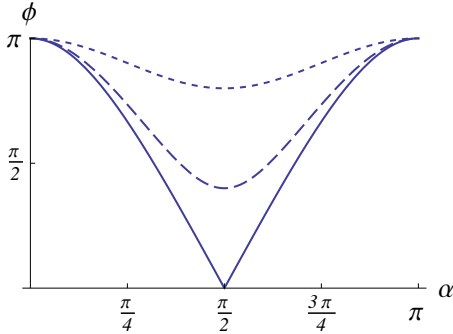


FIG. 5: The relation between the AB flux  $\phi$  and the Rashba SOI strength  $\alpha$  at full filtering [Eq. (46)]. The full line and the dashed lines with decreasing sized dashes correspond to the rhombus's opening angle  $\beta/\pi = .25, .15$  and  $.05$ . Results are the same under  $(\pi/4 - \beta) \leftrightarrow (\beta - \pi/4)$ .

When Eq. (46) is satisfied, the outgoing electrons are polarized along  $\hat{\mathbf{n}}'$ . The variation of the components of this polarization with  $\alpha$ , when one moves along the lines in Fig. 5, is shown in Fig. 6, which also shows the spin directions in the  $xz$ -plane for  $\beta = \pi/4$ . Changing the sign

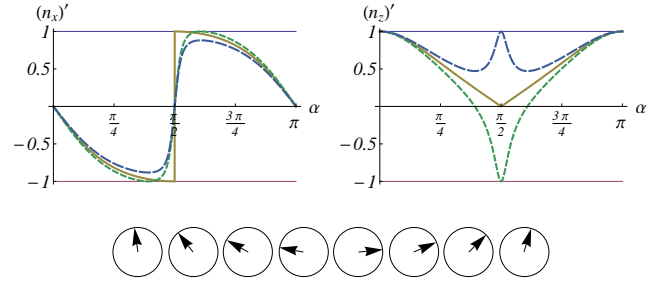


FIG. 6: The outgoing spin components for rhombus angles  $\beta = .25\pi, .23\pi$  and  $.27\pi$  (full line, small dashes and large dashes, respectively), as a function of the Rashba SOI strength  $\alpha$ , when the AB flux is given by Eq. (46). Changing  $\phi$  to  $-\phi$  switches the direction of the polarized spins. The lower panel shows the actual spin directions in the  $xz$ -plane for  $\beta = \pi/4$ , as  $\alpha$  increases from zero to  $\pi$  (left to right).

of  $\phi$  interchanges  $|\hat{\mathbf{n}}\rangle$  and  $|\hat{-\mathbf{n}}\rangle$ , and therefore changes the polarization associated with the blocked spinor from  $-\hat{\mathbf{n}}$  to  $\hat{\mathbf{n}}$ .

As Fig. 6 shows, at small  $\alpha$ , namely small electric field (and correspondingly large  $\phi$ , see Fig. 5) the outgoing spin points along the  $z$ -axis, parallel to the magnetic field. However, this spin ordering is not due to the Zeeman interaction, which is small (and neglected here), but rather due to the orbital effect of the AB flux. As  $\alpha$  increases, the spin rotates towards the negative  $x$ -direction. For  $\beta = \pi/4$ , the spin reaches this direction as  $\alpha \rightarrow \pi/2$ , and then flips abruptly to the opposite direction. Upon further increase of  $\alpha$ , the outgoing spin rotates back towards the positive  $z$ -direction. When  $\beta \neq \pi/4$ , the outgoing spin also rotates towards the positive  $x$ -direction, but now the results depend on  $\beta$ : when  $\beta < \pi/4$  ( $> \pi/4$ ) the spin continuously rotates towards the negative (positive)  $z$ -direction as  $\alpha \rightarrow \pi/2$ . These dips (peaks) in  $n'_z$  near  $\alpha = \pi/2$  become sharper as  $\beta$  approaches  $\pi/4$ .

As mentioned in the previous subsection, there is no filtering at exactly  $\alpha = \pi/2$  and  $\beta = \pi/4$ , namely at  $\phi = 0$ . However, the effect is most striking in the vicinity of  $\beta = \pi/4$ ,  $\alpha = \pi/2$  and  $\phi = 0$ . In fact, if one wishes to flip the outgoing spins by a small change in the electric field, which determines  $\alpha$ , then it would be best to use the filter for a small finite flux  $\phi$  and for  $\beta = \pi/4$ . Changing  $\alpha$  from  $\pi/2 - \phi\sqrt{2}/4$  to  $\pi/2 + \phi\sqrt{2}/4$  will cause a jump in  $n'_x$  from  $-1$  to  $1$ , i.e. a flip of the polarization from the negative to the positive  $x$ -direction. Alternatively, two filters with  $\beta > \pi/4$  and  $\beta < \pi/4$  would give opposite spin components near  $\alpha = \pi/2$  and the appropriate value of  $\phi$  as given by Eq. (46).

Since  $n_y = 0$ , the procedure outlined after Eq. (38) yields only the  $x$  and  $z$  components of the polarization of the incoming electrons,  $\hat{\mathbf{n}}_0$ . However, the third component can always be deduced from  $|\hat{\mathbf{n}}_0|^2 = 1$ . As discussed below, this issue is overcome when one adds the Dresselhaus SOI. Alternatively, we note that the vector

$\hat{\mathbf{n}}$  is in the  $xz$ -plane only when the diamond is placed as in Fig. 1, with the sites 0 and 1 on the  $x$ -axis. Placing these sites along the  $y$ -axis will place  $\hat{\mathbf{n}}$  in the  $yz$ -plane. Thus, splitting the incoming beam, which contains many electrons in identical spin states, into two beams, which go through two diamonds placed along the two axes, will allow a simultaneous determination of all the components of  $\hat{\mathbf{n}}_0$ .

So far, we applied Eq. (46) at fixed  $\beta$ , and obtained full filtering by varying both  $\phi$  and  $\alpha$  (namely the magnetic and electric fields) simultaneously. An alternative, which may be more attractive under some circumstances, is to vary  $\beta$  by moving the dots  $b$  and  $c$  towards the  $x$ -axis. As noted after Eq. (40), such motion also affects the area of the diamond and the length of each edge. Fixing the magnetic field fixes  $\phi_1$  [Eq. (41)], and Eq. (46) becomes

$$\alpha_1 = \pm \cos \beta \arccos[1 - 2 \cos(\phi_1 \tan \beta/2) / \sin(2\beta)] / 2. \quad (47)$$

The top panel in Fig. 7 shows this relation for four values of  $\phi_1$ . All four lines show a smooth monotonic variation of  $\alpha_1$  [i.e. the electric field responsible for  $k_R$ , Eq. (41)] with  $\beta$  (i.e. the electric field responsible for moving the dots  $b$  and  $c$ ), over ranges which become wider as  $\phi_1$  increases. The other panels in Fig. 7 show the two components of the polarized spin when Eq. (47) is obeyed. Varying  $\beta$  rotates this polarization. Setting the site energies so that the maximum of  $T_+$  is at  $\phi_0 = \phi_1$ , the transmission given in Eq. (37) remains close to unity over a range of  $\beta$  around  $\pi/4$ .

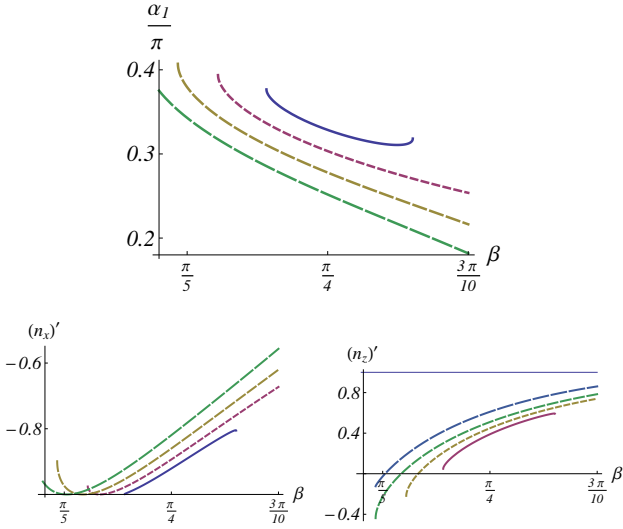


FIG. 7: Top: The relation between the strength of the Rashba SOI  $\alpha_1 = k_R L_0$  and the diamond angle  $\beta$  for full filtering, Eq. (47). Bottom: the two components of the outgoing polarized spins versus  $\beta$ . Full line and increasing dashes correspond to  $\phi_1 = .05, .1, .15$  and  $.2$ .

#### D. Single diamond with both Rashba and Dresselhaus SOI's

Since the Dresselhaus SOI [Eq. (3)] depends on the directions of the crystal axes, one needs to introduce the angles between the diamond bonds and these axes, as in Fig. 3. Thus,  $\mathbf{r}_0 = (0, 0, 0)$ ,  $\mathbf{r}_1 = 2L \cos \beta (\cos \nu, \sin \nu, 0)$ ,  $\mathbf{r}_b = L(\cos(\nu + \beta), \sin(\nu + \beta), 0)$ ,  $\mathbf{r}_c = L(\cos(\nu - \beta), \sin(\nu - \beta), 0)$ . We then use the vector  $\mathbf{K}$  from Eq. (4) and the AB phase from Eq. (39). Denoting also

$$\zeta^2 = \alpha_R^2 + \alpha_D^2, \quad \tan \theta = \alpha_D / \alpha_R, \quad (48)$$

one recovers Eqs. (40), with the replacement of  $\alpha$  by  $\zeta$  and with the new spin components  $\sigma_1 \equiv \sin \xi_1 \sigma_x - \cos \xi_2 \sigma_y$ ,  $\sigma_2 \equiv \sin \xi_4 \sigma_x + \cos \xi_3 \sigma_y$ , where  $\xi_1 \equiv \beta + \nu + \theta$ ,  $\xi_2 \equiv \beta + \nu - \theta$ ,  $\xi_3 \equiv \beta - \nu + \theta$ , and  $\xi_4 \equiv \beta - \nu - \theta$ .

Note that  $\sigma_1^2 = F_1^2 = 1 + \sin(2\nu + 2\beta) \sin(2\theta)$ ,  $\sigma_2^2 = F_2^2 = 1 + \sin(2\nu - 2\beta) \sin(2\theta)$ , and therefore  $e^{i\zeta\sigma_n} = c_n + i s_n \sigma_n$ , with  $c_n \equiv \cos(\zeta F_n)$ ,  $s_n \equiv \sin(\zeta F_n) / F_n$ . With these notations, one has

$$e^{i\zeta\sigma_1} e^{-i\zeta\sigma_2} = \delta + i\boldsymbol{\tau} \cdot \boldsymbol{\sigma}, \quad e^{-i\zeta\sigma_2} e^{i\zeta\sigma_1} = \delta + i\boldsymbol{\tau}' \cdot \boldsymbol{\sigma}, \quad (49)$$

where

$$\begin{aligned} \delta &= c_1 c_2 + s_1 s_2 (\sin \xi_1 \sin \xi_4 - \cos \xi_2 \cos \xi_3), \\ \tau_x &= \tau'_x = s_1 c_2 \sin \xi_1 - c_1 s_2 \sin \xi_4, \\ \tau_y &= \tau'_y = -s_1 c_2 \cos \xi_2 - c_1 s_2 \cos \xi_3, \\ \tau_z &= -\tau'_z = s_1 s_2 (\sin \xi_1 \cos \xi_3 + \cos \xi_2 \sin \xi_4), \end{aligned} \quad (50)$$

and  $\delta^2 + |\boldsymbol{\tau}|^2 = 1$  from unitarity. It is now straightforward to recover the matrix  $\mathbf{W}$  [Eq. (11)], with

$$d = a_+ \delta, \quad b_x = i a_+ \tau_x, \quad b_y = i a_+ \tau_y, \quad b_z = i a_- \tau_z, \quad (51)$$

and with  $a_{\pm}$  as given in Eq. (43). Again, Eq. (18) is used to recover Eq. (22), with the identifications  $\cos \omega = 1 - 2\tau_z^2$  and

$$\hat{\mathbf{n}} = (-\tau_y, \tau_x, \delta) / \sqrt{1 - \tau_z^2}. \quad (52)$$

The condition for full filtering, Eq. (33), now becomes

$$\cos(\phi/2) = \pm \tau_z = \pm s_1 s_2 \sin(2\beta) \cos(2\theta). \quad (53)$$

This is the main result of this subsection. One immediately notes the following. (a) This condition reduces to Eq. (46) when  $\alpha_D = 0$ . (b) When  $\alpha_R = 0$ , this condition also reduces to Eq. (46), with  $\alpha_D$  replacing  $\alpha_R$ . This is not surprising, since the two types of SOI are related via a unitary transformation. (c) When  $\alpha_D = \pm \alpha_R$  then  $\cos(2\theta) = 0$ , and therefore Eq. (53) yields  $\phi = \pi$ , i.e.  $\sin \phi = 0$ . As discussed following Eq. (34), there is no filtering in this case, and all electrons are fully reflected.

When both  $\alpha_D$  and  $\alpha_R$  have non-trivial values then all three components of  $\hat{\mathbf{n}}$  are non-zero, and therefore the



procedure outlined after Eq. (38) allows the determination of *all* the three components of  $\hat{\mathbf{n}}_0$  by measuring the charge transmission for three values of  $\hat{\mathbf{n}}$ . As mentioned, usually  $k_D$  is fixed for a given material and  $k_R$  can be varied experimentally by tuning the electric field in the  $z$  direction. At non-trivial values of  $k_D$ , the values of  $\phi$  for full filtering, Eq. (53), are no longer periodic in  $\alpha_R$ . An exception occurs for  $\nu = 0$  and  $\beta = \pi/4$  (see Fig. 3), when (53) reduces to

$$\pm \cos(\phi/2) = \sin^2 \alpha_R - \sin^2 \alpha_D. \quad (54)$$

Figure 8 shows this special periodic result for three values of  $\alpha_D$  (full and larger dashes). Interestingly, if  $\alpha_D = \pi/2$  then the curve for the pure Rashba SOI case just shifts to the left by  $\pi/2$ , so that the interesting regime moves to small electric and magnetic fields. However, other values of  $\alpha_D$  (e.g.  $\pi/4$  in the figure) give a much narrower range of  $\phi$ .

For all other values of  $\nu$  and  $\beta$  the flux  $\phi$  for full filtering is not periodic in  $\alpha_R$ , and one must use the full expression (53). This expression becomes simple for  $\nu = \beta = \pi/4$ ,

$$\pm \cos(\phi/2) = \sin^2 \zeta \cos(2\theta). \quad (55)$$

Figure 8 also shows this function (smallest dashes) for  $\alpha_D = \pi/4$ . As  $\alpha_R$  increases, this expression approaches the Rashba condition, Eq. (46), whereas Eq. (54) remains periodic in  $\alpha_R$ . As seen in the figure, working near  $\alpha_R = 3\pi/2$  already brings us close to the pure Rashba behavior. We trust that this value can be achieved with reasonable electric fields. Presumably, one can control the angle  $\nu$  by rotating the crystal which forms the filter.

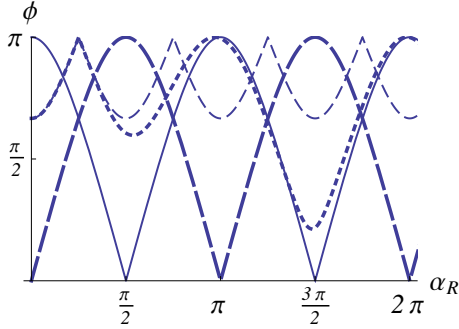


FIG. 8: Same as Fig. 5, with  $\beta = \pi/4$ ,  $\nu = 0$  (as defined in Fig. 3) and with the Dresselhaus SOI strength  $\alpha_D = 0$ ,  $\pi/4$  and  $\pi/2$  (full line, medium and long dashes respectively), Eq. (54). The line with the smallest dashes shows the filtering condition for  $\beta = \nu = \pi/4$  and  $\alpha_D = \pi/4$ , Eq. (55).

### III. TWO DIAMONDS

#### A. General formalism

Consider now two diamonds in series, connected at site 1 (Fig. 2, top). Eliminating the side sites ( $b$ ,  $c$ ,  $d$  and  $e$ ), we have

$$\begin{aligned} z_0|\psi(0)\rangle &= \mathbf{W}_A|\psi(1)\rangle - j|\psi(-1)\rangle, \\ z_2|\psi(2)\rangle &= \mathbf{W}_B^\dagger|\psi(1)\rangle - j|\psi(3)\rangle, \\ Z_1|\psi(1)\rangle &= \mathbf{W}_A^\dagger|\psi(0)\rangle + \mathbf{W}_B|\psi(2)\rangle, \end{aligned} \quad (56)$$

where  $z_0 = \epsilon - y_0$  [Eq. (9)],  $z_2 = \epsilon - \epsilon_2 - \gamma_{2d2} - \gamma_{2e2}$ ,  $Z_1 = \epsilon - \epsilon_1 - \gamma_{1b1} - \gamma_{1c1} - \gamma_{1d1} - \gamma_{1e1}$ ,  $\mathbf{W}_A$  represents Eq. (10) for diamond A and  $\mathbf{W}_B$  is defined similarly, with  $d, e$  replacing  $b, c$ . Eliminating site 1 then yields

$$\begin{aligned} (z_0 Z_1 \mathbf{1} - \mathbf{W}_A \mathbf{W}_A^\dagger)|\psi(0)\rangle &= \mathbf{W}_A \mathbf{W}_B |\psi(2)\rangle - Z_1 j |\psi(-1)\rangle, \\ (Z_1 z_2 \mathbf{1} - \mathbf{W}_B^\dagger \mathbf{W}_B)|\psi(2)\rangle &= \mathbf{W}_B^\dagger \mathbf{W}_A^\dagger |\psi(0)\rangle - Z_1 j |\psi(3)\rangle. \end{aligned} \quad (57)$$

Using the analogs of Eq. (12) for a wave coming from the left, and utilizing the identity

$$\mathbf{W}^\dagger [C\mathbf{1} + \mathcal{O}\mathbf{W}^\dagger]^{-1} \equiv [C\mathbf{1} + \mathbf{W}^\dagger \mathcal{O}]^{-1} \mathbf{W}^\dagger, \quad (58)$$

where  $\mathcal{O}$  and  $\mathbf{W}$  are arbitrary  $2 \times 2$  matrices and  $C$  is a number, yields for the transmission amplitude from left to right,

$$\begin{aligned} \mathcal{T} &= 2ij \sin(ka) \mathbf{W}_B^\dagger [Z_1 X_0 X_2 \mathbf{1} + X_0 \mathbf{W}_B \mathbf{W}_B^\dagger + X_2 \mathbf{W}_A^\dagger \mathbf{W}_A]^{-1} \mathbf{W}_A^\dagger \\ &= 2ij \sin(ka) \mathbf{W}_B^\dagger \frac{Z_1 X_0 X_2 + X_0 A_B + X_2 A_A - (X_0 \mathbf{B}_B + X_2 \mathbf{B}'_A) \cdot \boldsymbol{\sigma}}{(Z_1 X_0 X_2 + X_0 A_B + X_2 A_A)^2 - (X_0 \mathbf{B}_B + X_2 \mathbf{B}'_A)^2} \mathbf{W}_A^\dagger, \end{aligned} \quad (59)$$

where the second step uses Eqs. (17) and (27), with the corresponding coefficients  $A_{A,B}$ ,  $\mathbf{B}_{A,B}$  and  $\mathbf{B}'_{A,B}$ . Here,  $X_0$  was defined in Eq. (16), while similarly  $X_2 = \epsilon_2 + \gamma_{2d2} + \gamma_{2e2} + j e^{-ika}$ .

The factor  $\mathbf{W}_A^\dagger$  on the RHS implies that if we choose the parameters of  $A$  to produce full polarization then all the electrons entering from the left become fully polarized along  $\hat{\mathbf{n}}'_A$ , and the other factors in  $\mathcal{T}$  can be used to tune the unique polarization of the outgoing electrons, and perhaps the amplitude of the net transmission. Similarly, the factor  $\mathbf{W}_B^\dagger$  on the LHS means that if we tune  $B$  to

give full polarization then the outgoing electrons will all be polarized along  $\hat{\mathbf{n}}'_B$ , irrespective of the polarization of the incoming electrons.

We next consider two diamonds with an additional bond between them, see the lower panel in Fig. 2. The tight-binding equations are similar to the above, but now we also introduce a SOI on the bond between the sites 1 and 2,  $\tilde{U}_{12} = J_0 U$ , where  $U$  is a unitary matrix to be specified. Straightforward algebra, similar to that presented above, yields the left to right transmission amplitude

$$\mathcal{T} = -2ij \sin(ka) J_0 \mathbf{W}_B^\dagger U^\dagger [\Delta X_0 X_3 \mathbf{1} + z_1 X_0 U \mathbf{W}_B \mathbf{W}_B^\dagger U^\dagger + z_2 X_3 \mathbf{W}_A^\dagger \mathbf{W}_A + \mathbf{W}_A^\dagger \mathbf{W}_A U \mathbf{W}_B \mathbf{W}_B^\dagger U^\dagger]^{-1} \mathbf{W}_A^\dagger, \quad (60)$$

with  $\Delta = z_1 z_2 - J_0^2$ ,  $z_2 = \epsilon - \epsilon_2 - \gamma_{2d2} - \gamma_{2e2}$ ,  $X_0$  from Eq. (16) and  $X_3 = \epsilon_3 + \gamma_{3d3} + \gamma_{3e3} + j e^{-ika}$ .

Interestingly, one again has  $\mathbf{W}_A^\dagger$  on the RHS and  $\mathbf{W}_B^\dagger$  on the LHS. We expect this to be the case for any structure with these two diamonds at the ends. However, the present case differs from the previous one, since now  $\mathbf{W}_B$  appears only in the combination  $\tilde{\mathbf{W}}_B = U \mathbf{W}_B$ . Therefore one can use the unitary rotation of the spins  $U$  to modify the states which enter the diamond  $B$ , as discussed below.

### B. Ideal filtering

If both  $A$  and  $B$  are tuned to be full polarizers then one has

$$\mathbf{W}_A^\dagger = \sqrt{\lambda_{A+}} |\hat{\mathbf{n}}'_A\rangle \langle \hat{\mathbf{n}}_A|, \quad \mathbf{W}_B^\dagger = \sqrt{\lambda_{B+}} |\hat{\mathbf{n}}'_B\rangle \langle \hat{\mathbf{n}}_B| \quad (61)$$

and therefore Eq. (59) reduces to

$$\mathcal{T} = \frac{2ij \sin(ka) \langle \hat{\mathbf{n}}_B | \hat{\mathbf{n}}'_A \rangle \sqrt{\lambda_{A+} \lambda_{B+}}}{Z_1 X_0 X_2 + X_0 \lambda_{B+} + X_2 \lambda_{A+}} |\hat{\mathbf{n}}'_B\rangle \langle \hat{\mathbf{n}}_A|. \quad (62)$$

More generally, we can choose only one of the diamonds to fully polarize, and then we can tune the other one for optimization of the transmission and/or for tuning the polarization through the other diamond.

A particularly interesting possibility is to choose two identical diamonds, with  $\beta_A = \beta_B$ ,  $\epsilon_b = \epsilon_c = \epsilon_d = \epsilon_d$  and  $J_{uv} \equiv J$ . The only free parameters are now the two  $\phi$ 's and the strengths of the SOI's. Consider the pure Rashba case, and choose also  $\phi_A = \phi_B$  and  $\pi/2 - \alpha_A = \alpha_B - \pi/2$ , namely  $\sin(2\alpha_A) = -\sin(2\alpha_B)$ . With these choices one has  $A_A = A_B$  and  $\mathbf{B}_A = \mathbf{B}'_B$  [see Eqs. (44) and (45)]. In this case, the transmission amplitude is

$$\mathcal{T} = \frac{2ij \sin(ka) \lambda_+}{Z_1 X_0 X_2 + (X_0 + X_2) \lambda_+} |\hat{\mathbf{n}}_A\rangle \langle \hat{\mathbf{n}}_A|. \quad (63)$$

This device has the advantage that it fully transmits electrons with polarization along  $\hat{\mathbf{n}}_A$ , and does not rotate them as the single-diamond filter. Another important advantage involves the transmission. When  $Z_1$  is very small (but non-zero) and if also  $\epsilon \simeq 0$  and  $\epsilon_0 + 2\gamma_b = \epsilon_2 + 2\gamma_d = 0$  then the transmission of this polarized spin is close to unity for almost all  $\phi$ 's except for a narrow range near  $\phi = 0$  or  $\pi$  ( $\mathcal{T}$  still vanishes when  $\sin \phi = 0$ ). Moving away from the band center, the shape of the transmission  $T(\epsilon)$  depends on  $J$  and on  $\epsilon_b$ . For large enough  $J$ , the  $\gamma$ 's depend only weakly on  $\epsilon$ , and the transmission approaches the trivial value  $\sin^2(ka)$  ( $= 1$  in the band center), coming from the velocity of the electrons in the band. Thus, this structure is an ideal polarizer for energies close to the band center.

If we choose  $\mathbf{B}_A = -\mathbf{B}'_B$  then all the electrons will be blocked. For Rashba SOI, the latter condition implies the relations  $\hat{n}_{A,x} = \hat{n}_{B,x}$ ,  $\hat{n}_{A,z} = -\hat{n}_{B,z}$ , which can be realized if both  $\sin(2\alpha_A) = -\sin(2\alpha_B)$  and  $\phi_A = -\phi_B$  [Eqs. (22), (44)].

Finally, consider the second double diamond device, lower Fig. 2. Since  $U$  is unitary, the eigenvalues of  $\tilde{\mathbf{W}}_B \tilde{\mathbf{W}}_B^\dagger$  are the same as for  $\mathbf{W}_B \mathbf{W}_B^\dagger$ , namely  $\lambda_{B\pm}$ . However, the eigenstates are different:  $|\pm \hat{\mathbf{n}}_{BU}\rangle = U |\pm \hat{\mathbf{n}}_B\rangle$ . Using  $\mathbf{W}_A^\dagger$  from Eq. (61) and  $\tilde{\mathbf{W}}_B^\dagger = \sqrt{\lambda_{B+}} |\hat{\mathbf{n}}'_{BU}\rangle \langle \hat{\mathbf{n}}_{BU}|$ , Eq. (60) becomes  $\mathcal{T} = t |\hat{\mathbf{n}}'_{BU}\rangle \langle \hat{\mathbf{n}}_A|$ , with the transmission amplitude

$$t = \frac{-2ij \sin(ka) J_0 \langle \hat{\mathbf{n}}_{BU} | \hat{\mathbf{n}}'_A \rangle \sqrt{\lambda_{A+} \lambda_{B+}}}{\Delta X_0 X_3 + z_1 X_0 \lambda_{B+} + z_2 X_3 \lambda_{A+} + \lambda_{A+} \lambda_{B+}}. \quad (64)$$

The choices  $\epsilon_0 = \epsilon_1 = 2J^2/\epsilon_b = 2J^2/\epsilon_c$ ,  $\epsilon_2 = \epsilon_3 = 2J^2/\epsilon_d = 2J^2/\epsilon_e$ ,  $\hat{\mathbf{n}}_{BU} = \hat{\mathbf{n}}'_A$  and  $J_0 = 4J^4 \sin(\phi_{A0}) \sin(\phi_{B0}) / (j\epsilon_b \epsilon_d)$  yield a flat maximum of  $T = |t|^2$  at unity (similar to Fig. 4) for energies near the band center and fluxes near  $\phi_{A0}$  and  $\phi_{B0}$ . One can now tune the outgoing polarization via  $\mathbf{W}_A$ ,  $\mathbf{W}_B$  and/or  $U$ . Specifically, one has maximal transmission if one tunes the outgoing polarization to be along  $\hat{\mathbf{n}}_A$  by requiring

that  $U|\hat{\mathbf{n}}'_B\rangle = |\hat{\mathbf{n}}'_{BU}\rangle = |\hat{\mathbf{n}}_A\rangle$ . In the Rashba case, the vectors  $\hat{\mathbf{n}}_{A,B}$  and  $\hat{\mathbf{n}}'_{A,B}$  are both in the  $xz$ -plane, and therefore  $U = \exp[i\alpha_{12}\sigma_y]$ , where  $2\alpha_{12} = \arcsin([\hat{\mathbf{n}}_B \times \hat{\mathbf{n}}'_A]_y)$ . This rotation can be generated by an electric field in the  $z$ -direction, and its magnitude  $\alpha_{12}$  can also be changed by changing the length of the bond 12. Since the two diamonds fully polarize the electrons, and the intermediate bond can rotate their polarization, this device can perform as the Datta-Das SFET.

#### IV. SUMMARY AND DISCUSSION

We have demonstrated that single- and double-diamond devices, made of materials with strong SOI's, can act as both a spin filter and a spin analyzer. Our calculations includes the following specific achievements:

- Full filtering through a general single-loop interferometer requires a symmetry between the two branches ( $\gamma_b = \gamma_c$ ) and a relation between the AB phase and the SOI phase ( $\phi = \omega + \pi$ ). For the diamonds in Fig. 1 and in Fig. 3 these conditions and the direction of the filtered polarization  $\hat{\mathbf{n}}'$  can be independent of the electron's energy.

- The site energies and the hopping strengths around the diamond can be chosen so that the transmission  $T$  of the polarized electrons is close to unity over a wide range of energies and AB flux (Fig. 4).

- The charge transmission of polarized spins through the interferometer measures the angle between the directions of this incoming polarization  $\hat{\mathbf{n}}_0$  and that characterizing the full transmission by the filter, Eq. (38), rendering a reading of the former polarization.

- For the Rashba SOI, one can work at small magnetic fluxes, and generate a flipping of the transmitted polarization by a small change in the electric field (Fig. 6). One can also tune the transmitted polarization keeping the magnetic field fixed, and varying the shape of the diamond (Fig. 7).

- Adding the Dresselhaus SOI usually breaks the periodicity in the Rashba SOI strength  $k_R$  of the filtering criterion, and complicates the various expressions. However, increasing  $k_R$  brings the various expressions back to the pure Rashba ones.

- The two-diamond device can be tuned to be symmetric, so that the polarization of the electrons exiting the two-diamond device is equal to that of the incoming ones (from either side), with a transmission close to unity.

- Adding a bond with a SOI between the two diamonds allows tuning of the polarization of the spins. This adds much flexibility in the choice of the two diamonds. Since each diamond acts as a full filter, this double-diamond device achieves the aims of the Datta-Das SFET without ferromagnetic leads.

Are there materials for which one can reach values of  $\alpha_R$  or order  $\pi/2$ , as required here? A Shubnikov-de Haas experiment<sup>66</sup> on an  $\text{Al}_{0.25}\text{In}_{0.75}\text{As}$  barrier layer gave a value for the Rashba coefficient (in different units)  $\alpha =$

$3 \times 10^{-11}\text{eV/m}$ . With the effective mass  $m^* = 0.023m_0$ , this gives  $k_R = m^*\alpha/\hbar^2 = 9 \times 10^6\text{m}^{-1}$ . Weak antilocalization measurements in a quaternary  $\text{InGaAsP/InGaAs}$  heterointerface<sup>67</sup> yielded  $\alpha = 10.4 \times 10^{-12}\text{eVm}$ . With an effective mass  $m^* = 0.0408m_0$ , this gives  $k_R = 5.55 \times 10^6\text{m}^{-1}$ . Thus,  $L = 300\text{nm}$  would imply  $\alpha_R \sim 1.6 - 2.7$ , allowing for  $\alpha_R = \pi/2$ .

As in most of our references, we calculated only the *transmission* from left to right (or from right to left). Indeed, the results for the transmission describe the outcome of *scattering experiments*, when one has a beam of electrons coming in only from one side of the device. In many experiments, one would like to measure the *conductance* between these two sides, which involves the difference between a current coming from the left and a current coming from the right, as originally discussed by Landauer.<sup>68</sup> A generalization of this approach for our case has the form<sup>69</sup>

$$I^j = \int \frac{d\epsilon}{2\pi} [f_L(\epsilon) - f_R(\epsilon)] \text{Tr}[\mathcal{T}\mathcal{T}^\dagger \sigma_j], \quad (65)$$

where  $f_{L,R}(\epsilon) = 1/[1 + e^{(\epsilon - \mu_{L,R})/k_B T}]$  is the Fermi distribution function in the left  $L$  or right  $R$  reservoir,  $T$  is the temperature, and  $\mu_{L,R}$  are the chemical potentials on the electronic reservoirs connected to the leads). Denoting  $\sigma_0 = 1$ ,  $I^0$  gives the net charge current in units of  $e/h$ . Denoting the Pauli matrices by  $\sigma_j$ ,  $j = 1, 2, 3$ , the corresponding vector  $\mathbf{I} \equiv (I^1, I^2, I^3)$  gives the net spin current in the leads. In all of our examples, the hermitian matrix  $\mathcal{T}\mathcal{T}^\dagger$  can be written as  $\mathcal{T}\mathcal{T}^\dagger = T_+|\hat{\mathbf{n}}'\rangle\langle\hat{\mathbf{n}}'| + T_-|\hat{\mathbf{n}}'\rangle\langle-\hat{\mathbf{n}}'|$ , where  $\hat{\mathbf{n}}'$  denotes the polarization of the outgoing electrons [see Eq. (30)]. Therefore, at linear response and at zero temperature the charge conductance is given by  $(e^2/h)(T_+ + T_-)$ , and the spin conductance is  $\mathbf{I} = (T_+ - T_-)\hat{\mathbf{n}}'$ . When  $T_- = 0$ , both currents are associated with  $T_+$ , and the current is *fully polarized* even at linear response. When  $\phi \pm \omega = \pi/2$  then  $T_+ = T_- = T_0$ , and the current is not polarized at all. In this latter case the linear charge conductance is  $2e^2T_0/h$ , which could reach the full quantum value of  $2e^2/h$ .

Finite temperatures or bias voltages  $eV = \mu_L - \mu_R$  require summing of  $T_+(\epsilon)$  over energies. As noted, such sums do not affect the condition for full filtering or the direction of outgoing polarization. Furthermore, a flat energy dependence, as in Fig. 4, maintains a large conductance even after the summation is carried over. This generalized Landauer formula still gives only the currents between the two electron reservoirs, which have *unpolarized* electrons. Therefore, the results are not sensitive to the polarization of the incoming electrons, and a device based on connecting two unpolarized reservoirs cannot function as a spin analyzer. The situation changes for polarized reservoirs, but this requires more research.

Our calculations were restricted to one-dimensional bonds between the quantum dots. Real quantum wires may have a finite width. Although one still has only a few relevant channels,<sup>70</sup> their effect requires more analysis. In any case, the number of channels can also be

tuned by the gate voltages.

A major question, relevant to all filters, concerns the experimental verification that the outgoing spins are indeed fully polarized. One way to test this is to use the double-diamond device, as discussed in Sec. III. Switching from full transmission to no transmission by switching the sign of the magnetic field on the second diamond will supply a proof that the electrons have been polarized. An alternative way is to introduce a quantum dot with a strong Coulomb interaction on or near the outgoing lead.<sup>18,19</sup> Starting with no occupation on this dot, and then increasing the gate voltage on it to capture one electron from the polarized flow, will block the current due to Pauli's principle. Yet another method detects the

polarized current in quantum-point contacts via transverse electron focusing.<sup>71</sup>

### Acknowledgments

We acknowledge discussions with Y. Imry. AA and OEW acknowledge the hospitality of NTT and of the ISSP, where this project started, and support from the ISF and from the DIP. YT, AA and OEW also acknowledge support at NTT from the Funding Program for World-Leading Innovative R and D on Science and Technology (FIRST).

- 
- \* Electronic address: aaharony@bgu.ac.il; Also at Tel Aviv University.
- † Also at Tel Aviv University.
- <sup>1</sup> S. A. Wolf, D. D. Awschalom, R. A. Buhrman, J. M. Daughton, S. von Molnár, M. L. Roukes, A. Y. Chtchelkanova, and D. M. Treger, *Science* **294**, 1488 (2001).
  - <sup>2</sup> M. A. Nielsen and I. L. Chuang, *Quantum Computation and Quantum Information* (Cambridge Univ. Press, Cambridge, 2011).
  - <sup>3</sup> D. Loss and D. P. DiVincenzo, *Phys. Rev. A* **57**, 120 (1998).
  - <sup>4</sup> F. H. L. Koppens, C. Buizert, K. J. Tielrooij, I. T. Vink, K. C. Nowack, T. Meunier, L. P. Kouwenhoven, and L. M. K. Vandersypen, *Nature* **442**, 766 (2006).
  - <sup>5</sup> M. Pioro-Ladriere, T. Obata, Y. Tokura, Y. -S. Shin, T. Kubo, K. Yoshida, T. Taniyama, and S. Tarucha, *Nature Physics*, **4**, 776 (2008).
  - <sup>6</sup> C. H. W. Barnes, J. M. Shilton, and A. M. Robinson, *Phys. Rev. B* **62**, 8410 (2000).
  - <sup>7</sup> A. E. Popescu and R. Ionicioiu, *Phys. Rev. B* **69**, 245422 (2004).
  - <sup>8</sup> J. Ebbecke, G. Bastian, M. Blocker, K. Pierz, and F. J. Ahlers, *Appl. Phys. Lett.* **77**, 2601 (2000).
  - <sup>9</sup> T. Hayashi, T. Fujisawa, H. D. Cheong, Y. H. Jeong, and Y. Hirayama, *Phys. Rev. Lett.* **91**, 226804 (2003).
  - <sup>10</sup> B. T. Jonker, G. Kioseoglou, A. T. Hanbicki, C. H. Li, and P. E. Thompson, *Nature Physics* **3**, 542 (2007).
  - <sup>11</sup> A. Oiwa, Y. Mitsumori, R. Moriya, T. Shupinski, and H. Munekata, *Phys. Rev. Lett.* **88**, 137202 (2002).
  - <sup>12</sup> I. Žutić, J. Fabian, and S. Das Sarma, *Rev. Mod. Phys.* **76**, 323 (2004).
  - <sup>13</sup> P. LeClair, J. K. Ha, H. J. M. Swagten, J. T. Kohlhepp, C. H. van de Vin, and W. J. M. de Jonge, *Appl. Phys. Lett.* **80**, 625 (2002).
  - <sup>14</sup> T. S. Santos, J. S. Moodera, T. S. Santos, and J. S. Moodera, *Phys. Rev. B* **69**, 241203(R) (2004).
  - <sup>15</sup> M. Gajek, M. Bibes, A. Barthélémy, K. Bouzehouane, S. Fusil, M. Varela, J. Fontcuberta, and A. Fert, *Phys. Rev. B* **72**, 020406(R) (2005).
  - <sup>16</sup> U., Lüders, M. Bibes, K. Bouzehouane, E. Jacquet, J.-P. Contour, S. Fusil, J.-F. Bobo, J. Fontcuberta, A. Barthélémy, and A. Fert, *Appl. Phys. Lett.* **88**, 082505 (2006).
  - <sup>17</sup> P. Recher, E. V. Sukhorukov, and D. Loss, *Phys. Rev. Lett.* **85**, 1962 (2000).
  - <sup>18</sup> T. Otsuka, E. Abe, Y. Iye, and S. Katsumoto, *Phys. Rev. B* **79**, 195313 (2009).
  - <sup>19</sup> K. Ono, D. G. Austing, Y. Tokura, and S. Tarucha, *Science* **297**, 1313 (2002).
  - <sup>20</sup> J. A. Folk, R. M. Potok, C. M. Marcus, and V. Umansky, *Science* **299**, 679 (2003).
  - <sup>21</sup> R. Hanson, L. M. K. Vandersypen, L. H. Willems van Beveren, J. M. Elzerman, I. T. Vink, and L. P. Kouwenhoven, *Phys. Rev. B* **70**, 241304(R) (2004).
  - <sup>22</sup> S. Datta and B. Das, *Appl. Phys. Lett.* **56**, 665 (1990).
  - <sup>23</sup> J. J. Sakurai, *Modern Quantum Mechanics* (Addison Wesley, Boston, 1994), p. 304.
  - <sup>24</sup> R. Winkler, *Spin-Orbit Coupling Effects in Two-Dimensional Electron and Hole Systems* (Springer-Verlag, Berlin, 2003).
  - <sup>25</sup> E. I. Rashba, *Fiz. Tverd. Tela (Leningrad)* **2**, 1224 (1960) [*Sov. Phys. Solid State* **2**, 1109 (1960)]; Y. A. Bychkov and E. I. Rashba, *J. Phys. C* **17**, 6039 (1984).
  - <sup>26</sup> J. Nitta, T. Akazaki, H. Takayanagi, and T. Enoki, *Phys. Rev. Lett.* **78**, 1335 (1997); T. Koga, J. Nitta, T. Akazaki, and H. Takayanagi, *Phys. Rev. Lett.* **89**, 046801 (2002).
  - <sup>27</sup> M. König, A. Tschetschetkin, E. M. Hankiewicz, J. Sinova, V. Hock, V. Daumer, M. Schäfer, C. R. Becker, H. Buhmann, and L. W. Molenkamp, *Phys. Rev. Lett.* **96**, 076804 (2006).
  - <sup>28</sup> T. Bergsten, T. Kobayashi, Y. Sekine, and J. Nitta, *Phys. Rev. Lett.* **97**, 196803 (2006).
  - <sup>29</sup> T. Koga, Y. Sekine, and J. Nitta, *Phys. Rev. B* **74**, 041302 (2006).
  - <sup>30</sup> G. Dresselhaus, *Phys. Rev.* **100**, 580 (1955).
  - <sup>31</sup> E. I. Rashba and V. I. Sheka, in *Landau Level Spectroscopy*, edited by G. Landwehr and E. I. Rashba (Elsevier, Amsterdam, 1991).
  - <sup>32</sup> Y. Oreg and O. Entin-Wohlman, *Phys. Rev. B* **46**, 2393 (1992).
  - <sup>33</sup> M. Khodas, A. Shekhter, and A.M. Finkel'stein, *Phys. Rev. Lett.* **92**, 086602 (2004).
  - <sup>34</sup> A. Shekhter, M. Khodas, and A. M. Finkel'stein, *Phys. Rev. B* **71**, 125114 (2005).
  - <sup>35</sup> J. Linder, T. Yokoyama, and A. Sudbø, *Phys. Rev. B* **81**, 075312 (2010).
  - <sup>36</sup> M. Yamamoto, J. Ohea, T. Ohtsuki, J. Nitta, and B. Kramer, *Physica E* **29**, 490 (2005).

- <sup>37</sup> M. Yamamoto, T. Ohtsuki, and B. Kramer, *Phys. Rev. B* **72**, 115321 (2005).
- <sup>38</sup> M. Yamamoto, K. Dittmer, B. Kramer, and T. Ohtsuki, *Physica E* **32**, 462 (2006).
- <sup>39</sup> T. Yokoyama and M. Eto, *Physica E* **42**, 956 (2010).
- <sup>40</sup> Y. Aharonov and D. Bohm, *Phys. Rev.* **115**, 485 (1959).
- <sup>41</sup> M. V. Berry, *Proc. R. Soc. London A* **392**, 45 (1984).
- <sup>42</sup> Y. Aharonov and A. Casher, *Phys. Rev. Lett.* **53**, 319 (1984).
- <sup>43</sup> Y. Meir, Y. Gefen, and O. Entin-Wohlman, *Phys. Rev. Lett.* **63**, 798 (1989).
- <sup>44</sup> A. G. Aronov and Y. B. Lyanda-Geller, *Phys. Rev. Lett.* **70**, 343 (1993).
- <sup>45</sup> J. Nitta, F. E. Meijer, and H. Takanayagi, *Appl. Phys. Lett.* **75**, 695 (1999).
- <sup>46</sup> B. Molnár, F. M. Peeters, and P. Vasilopoulos, *Phys. Rev. B* **69**, 155335 (2004).
- <sup>47</sup> D. Frustaglia, and K. Richter, *Phys. Rev. B* **69**, 235310 (2004).
- <sup>48</sup> R. Citro, F. Romero and M. Marinaro, *Phys. Rev. B* **74**, 115329 (2006).
- <sup>49</sup> V. Marigliano Ramaglia, V. Cataudella, G. De Filippis, and C. A. Perroni, *Phys. Rev. B* **73**, 155328 (2006).
- <sup>50</sup> M. J. van Veenhuizen, T. Koga, and J. Nitta, *Phys. Rev. B* **73**, 235315 (2006).
- <sup>51</sup> N. Hatano, R. Shirasaki, and H. Nakamura, *Phys. Rev. A* **75**, 032107 (2007).
- <sup>52</sup> P. Földi, O. Kálmán, M. G. Benedict, and F. M. Peeters, *Phys. Rev. B* **73**, 155325 (2006).
- <sup>53</sup> F. Chi and J. Zheng, *Appl. Phys. Lett.* **92**, 062106 (2008).
- <sup>54</sup> S-H Chen and C-R Chang, *Phys. Rev. B* **77**, 045324 (2008).
- <sup>55</sup> R. Ionicioiu and I. D'Amico, *Phys. Rev. B* **67**, 041307(R) (2003).
- <sup>56</sup> T. Koga, J. Nitta, and M. van Veenhuizen, *Phys. Rev. B* **70**, 161302 (2004).
- <sup>57</sup> U. Zuelicke, *Appl. Phys. Lett.* **85**, 2616 (2004).
- <sup>58</sup> U. Zuelicke and A. I. Signal, *Solid State Commun.* **144**, 529 (2007).
- <sup>59</sup> A. López, E. Medina, N. Bolívar, and B. Berche, *J. Phys.: Condens. Matter* **22**, 115303 (2010).
- <sup>60</sup> B. Molnár, P. Vasilopoulos, and F. M. Peeters, *Phys. Rev. B* **72**, 075330 (2005).
- <sup>61</sup> D. Bercioux, M. Governale, V. Cataudella, and V. Marigliano Ramaglia, *Phys. Rev. B* **72**, 075305 (2005).
- <sup>62</sup> A. Aharony, O. Entin-Wohlman, Y. Tokura, and S. Katsumoto, *Phys. Rev. B* **78**, 125328 (2008).
- <sup>63</sup> A. Aharony, O. Entin-Wohlman, Y. Tokura, and S. Katsumoto, *Physica E* **42**, 629 (2009).
- <sup>64</sup> O. Kálmán, T. Kiss, and P. Földi, *Phys. Rev. B* **80**, 035327 (2009).
- <sup>65</sup> C. W. J. Beenakker, *Rev. Mod. Phys.* **69**, 731 (1997).
- <sup>66</sup> D. Grunder, *Phys. Rev. Lett.* **84**, 6074 (2000).
- <sup>67</sup> M. Kohda and J. Nitta, *Phys. Rev.* **81**, 115118 (2010).
- <sup>68</sup> R. Landauer, *Phil. Mag.* **21**, 863 (1970).
- <sup>69</sup> O. Entin-Wohlman, A. Aharony, Y. Tokura, and Y. Avishai, *Phys. Rev. B* **81**, 075439 (2010).
- <sup>70</sup> A. Aharony, O. Entin-Wohlman, T. Otsuka, S. Katsumoto, H. Aikawa, and K. Kobayashi, *Phys. Rev. B* **73**, 195329 (2006).
- <sup>71</sup> A. Reynoso, G. Usaj, and C. A. Balseiro, *Phys. Rev. B* **75**, 085321 (2007).